# *Magnetic silica nanoparticles for use in matrix-assisted laser desorption ionization mass spectrometry of labile biomolecules such as oligosaccharides, amino acids, peptides and nucleosides*

# Magnetic silica nanoparticles for use in matrix assisted laser desorption ionization mass spectrometry of labile biomolecules such as oligosaccharides, amino acids, peptides and nucleosides

**Hongmei Yang[1,2] · Rui Su[1] · John S. Wishnok[2] · Ning Liu[3,4] · Changbao Chen[1] · Shuying Liu[1] · Steven R. Tannenbaum[2,5]**

[1] Changchun University of Chinese Medicine, Changchun 130117, China

[2] Department of Biological Engineering, Massachusetts Institute of Technology, Cambridge, MA 02139, United States

[3] Central Laboratory, The Second Hospital of Jilin University, Changchun 130041, China

[4] Key Laboratory of Zoonosis Research, Ministry of Education, Jilin University, Changchun 130062, China

[5] Department of Chemistry, Massachusetts Institute of Technology, Cambridge, MA 02139

Corresponding authors. E-mail: srt@mit.edu; liu_ning@jlu.edu.cn

Keywords: Soft matrix · Small thermal labile biomolecules · Little or no fragmentation · High salt tolerance · Reduced chemical background · Ultrahigh sensitivity · Reliable quantitative assay · LDI MS

**Abstract**

Magnetic silica nanoparticles (MSNPs) were prepared and applied for the first time as a matrix in MALDI MS for analysis of small thermal labile biomolecules including oligosaccharides, amino acids, peptides, nucleosides, and gensenosides. The matrix was characterized by scanning electron microscopy and UV-vis spectroscopy. It displays good performance in analyses of such biomolecules in the positive ion mode. In addition, the method generates significantly less energetic ions compared to the use of carbon nanotubes or graphene-assisted LDI MS and thus produces intact molecular ions with little or no fragmentation. In addition, the MSNPs have better surface homogeneity and better salt tolerance and cause lower noise. It is assumed that the soft ionization observed when using MSNPs as a matrix is due to the specific surface area and the homogenous surface without large clusters. The matrices were applied to the unambiguous identification and relative quantitation of the water extract of *Panax ginseng* roots. Any false-positive results as obtained when using graphene and carbon nanotubes as a matrix were not observed.

## Introduction

Small molecules, including oligosaccharides, peptides, natural products, and receptor ligands play important roles in multiple biological processes [1-3]. One of the main current techniques for small molecular analysis is liquid chromatography-mass spectrometry (LC-MS). It has some limitations such as matrix effects and the unavoidable loss of pathological information or active ingredients during sample preparation [4,5]. Progress in research can be hindered by analytical limitations, which often demands rapid and direct analysis as well as high-throughput sample screening. Matrix-assisted laser desorption ionization mass spectrometry (MALDI-MS) has achieved great success in the rapid analysis of biomacromolecules (DNA, proteins, polypeptides, polymers etc.) [6,7]. Typically an organic matrix is used to facilitate the ionization of macromolecules, but detection of small molecules (<700 Da) has been a challenge in MALDI MS due to interference from conventional matrices in the low mass region [8-10].

To circumvent the matrix-related background interference problem, much effort has been made in the last decade to explore interference-free methods. Possible approaches include designing higher-molecular-weight organic matrices, introducing ion liquid matrices, and selecting additives for matrices, etc. [11,12] Although reduced chemical background in the low *m/z* region has been often observed, none were background-free. An attractive alternative approach is to develop nanomaterial-based matrices. A variety of nanostructured surfaces and nanomaterials, such as silicon and platinum nanostructured surfaces, gold, silver, platinum, graphene, silica, thymine chitosan

nanomagnets, and magnesium oxide nanoparticles (NPs), have been applied as alternative matrices for MALDI to minimize low *m/z* interferences [13-20]. Graphene nanoflakes assisted LDI-MS was an efficient tool for research in lipidomics of cancer cells and cancer stem cells [15]. Compared to traditional matrices, NPs generate little background signal in the <700 Da region. However, abundant fragments have been reported from lipids, oligosaccharides, and other organic compounds using gold nanoparticles [21-23], a glutathione-capped iron oxide nanoparticle matrix [24], colloidal graphite [25], and silicon nanowires [26,27] as matrices. It therefore remains a challenge to distinguish the signals from endogenous analytes in complex samples from those resulting from degradation or dissociation of the analytes themselves.

In comparison, relatively little has been done to explore how nanomaterials might reduce fragmentation. This gap in methodology inspired us to develop soft and cost-effective NPs for future biomedical research. Magnetic nanoparticles have gained wide interest on account of their good biocompatibility and low toxicity in diverse fields such as affinity-based analysis, protein separation and drug delivery [28,29]. In the present study, a magnetic silica nanoparticle (MSNP) was used as a novel and versatile MALDI matrix for analysis of a broad range of small molecules. The principal aim of this study was to confirm the ability of MSNP as a soft matrix for efficient detection of the labile compounds including nonreducing oligosaccharides and nucleosides by MALDI time of flight (TOF) MS. In comparison to the common used NPs, MSNPs allowed for high salt tolerance, fast detection of small molecules with a clean background in the low mass-to-charge (*m/z*) regions of the spectra, and ultrahigh sensitivity (limit of detection

(LOD) ≈ 5 fmol). Successful quantitative MALDI performance of this new matrix was also demonstrated for berberine and palmatine. Finally, using the water-soluble ginseng extract as a model system, the present method demonstrated a promising tool for fast and unambiguous analysis of small molecules in real samples. Overall, this work represents a new way where MSNPs can be exploited to improve biomedical analysis.

## Experimental section

### Chemicals and reagents

Ferrofluid EMG 911 was purchased from Ferrotech (Nashua, NH, https://www.ferrotec.com/). Raffinose, sucrose, and 2′-deoxycytidine were acquired from Aladdin (Shanghai, China, http://www.aladdin-e.com/). Berberine, jatrorrhizine, and palmatine were obtained from the National Institute for the Control of Pharmaceutical and Biological Products (Beijing, China, http://www.nicpbp.org.cn/CL0263/). Carbon nanotubes and graphene were provided by Shenzhen Nanotech Port Co., Ltd. (Shenzhen, China, https://cnanotube.en.ec21.com/). The roots of *P.* ginseng were cultivated and collected from Changbai Mountain (Jilin, China). All other chemicals (analytical grade) were bought from Sigma-Aldrich (St. Louis, MO, https://www.sigmaaldrich.com/united-states.html) and were used without further purification. Ultrapure water (specific conductivity, 18.2 MΩ/cm) was produced by a MilliQ device (Millipore, Eschborn, Germany, http://www.merckmillipore.com/CN/zh).

### Synthesis and characterization of MSNPs

MSNPs were synthesized based on a previously reported protocol with some

modifications [30,31]. The detailed synthesis procedure was described in the Supporting Information. The morphology and size of the MSNPs were studied using a scanning electron microscope (SEM) (XL30ESEM-FEG, FEI Co., USA) operated at an accelerating voltage of 25 kV. The UV−vis spectrum was collected on a UV-1102II ultraviolet spectrophotometer (Techcomp (China) Ltd., China) equipped with a quartz colorimetric vessel of 1-cm path length.

**Matrix solutions and sample preparation for MALDI MS**

MNSPs, carbon nanotubes, and graphene (2 mg) were suspended individually with 1 mL of ethanol/water (95:5, v/v) and sonicated for 2 min, in which the nanoparticles can be well-dispersed. To obtain the best performance, four different matrix deposition strategies were tested, and the detailed procedure was described in the Supporting Information.

**Surface-assisted laser desorption ionization (SALDI)-MS analysis**

All mass spectra were recorded on a MALDI-TOF-TOF mass spectrometer (Ultraflex Bruker Daltonics, Bremen, Germany) equipped with a Nd:YAG laser (355 nm). The instrument was operated in positive ion, reflectron mode. The accelerating voltage was set at 20 kV, and the delay time was set at 100 ns. The laser was fired at a frequency of 100 Hz, and spectra were recorded from the sum of 100 laser shots. All depicted spectra were calibrated using an external calibration equation generated from the ion signals of a mixture of raffinose (527.16 Da), verbascose (851.26 Da), and CHCA (190.05 Da).

**Results and discussion**

**Characterization of the MSNPs**

The obtained nanoparticles were characterized using SEM to obtain information on size, shape, and distribution on a solid support, and ultraviolet spectrophotometer to test UV−vis absorption ability. The SEM image in Fig. 1a clearly indicates that the final colloids are fairly uniform in size and shape, with a mean diameter of 200 ± 30 nm (n=100). One crucial prerequisite for a compound to be an appropriate matrix is a strong absorbance at a certain laser wavelength. As shown in Fig. 1b, the nanoparticles exhibit a strong absorption below 450 nm, which is within the optimal range of the MALDI laser (355 nm) used in the mass spectrometry experiments and should serve as efficient MALDI matrices to absorb and transfer laser energy. The good properties of MSNPs may be attributed to the specific surface area of MSNPs, and the suspension of MSNPs was mainly colloidal rather than being a transparent solution.

**Evaluation of the properties of MSNP as matrix**

The presence of ‘hot’ and ‘cold’ sites within a MALDI spot limited spot-to-spot reproducibility and made data acquisition lengthier and more difficult. Thus, the ability to obtain signals from the entire sample area without the need to search for hot or cold spots is very important. The morphology of the crystal layer resulting from sample deposition in MSNPs when analyzing raffinose by the sample-first method is shown in Fig. 2a. This sample preparation method was used to analyze small molecules in this study because it offered significant advantages (Fig. S1) over the other three ones as described in **Sample Preparation for MALDI MS** in the Supporting Information. The advantages included the improvement of signal to noise ratio (S/N), resolution, and the signal intensity. What's the role of iron oxide nanoparticles in MALDI determination of

small biomolecules? On the one hand, the size of the iron oxide–silica colloids can be controlled by varying the concentrations of iron oxide nanoparticles. In addition, iron oxide nanoparticles have the organophilic behavior [30]. Thus, it is inferred that this behavior is favorable to the cocrystallization between organic analytes and MSNPs. In case of silica, it plays an important role in absorbing laser energy and transfering energy to analytes [26,27]. A very homogenous surface without large clusters was obtained (Fig. 2a), which suggests the even distribution of 'hot' sites that may help to reduce the MALDI signal fluctuation.

To evaluate the spot-to-spot reproducibility with MSNPs as matrices, a set of experiments with a sample concentration of 0.1 mg/mL glucose was conducted using 50 different sample spots. The relative standard deviation (RSD) for the signal intensity was below 15%, indicating that no 'sweet spot' problem arises, which is the most critical factor for accurate and robust quantification. Therefore, we further investigated the use of matrix-free MSNPs for quantitative measurement in MALDI-TOF MS. The quantitative standard plots of berberine and palmatine, which are two bioactive alkaloids in traditional Chinese medicines, were established with the use of jatrorrhizine which has a similar structure as an internal standard using MSNP matrix. Excellent linearities ($R^2$ = 0.9918 for palmatine and $R^2$ = 0.9928 for berberine, 20-1000 fmol/μL) were obtained between the signal intensity ratios (berberine/jatrorrhizine and palmatine/jatrorrhizine) and analyte concentrations, demonstrating that MSNPs provided a rapid, and reliable quantitative assay for small molecules (Fig. 2b). In addition, the detection limits for berberine, jatrorrhizine, and palmatine are around 5

fmol with S/N $\approx$ 5, indicating ultrahigh sensitivity (5 fmol) assisted by MSNP matrix for small-molecule analysis.

High concentrations of salts will seriously suppress the signal of the analytes and lead to poor ionization efficiency. The salt-tolerance ability of a matrix is also an important factor which affects its application in complex samples. A mixture of glutamine (70 ppm), glucose (100 ppm), 2′-deoxycytidine (5 ppm), carbetamide (10 ppm), a dipeptide (Asp-Leu) (70 ppm), and kojibiose (50 ppm) was selected to evaluate the salt tolerance capability of MSNPs. As depicted in Fig. 3, the six compounds can be detected with good S/N in the presence of 2 M NaCl, 2 M $NH_4CO_3$ and 2 M urea. The ions marked in blue were assigned as potassium-associated ions, and the black ones are sodium-coordinated ions. Through the addition of NaCl, disodium (the ions at *m/z* 191.05 and 291.24) and trisodium (the ion at *m/z* 313.23) cationized ions were observed (Fig. 3a). In the case of the purple-labelled ions, they corresponded to $[DL + Na + K - H]^+$ (Fig. 3b and c). Under the same conditions, no signals or bad signals were detected using graphene and carbon nanotubes as matrices (data not shown). These results demonstrated that MSNPs have a high salt tolerance and a promising potential application for analysis of small molecules in complex biological samples.

It is important that we choose a matrix which does not interfere with analyte detection. To investigate this behavior of MSNPs for MALDI TOF-MS analysis, comparative studies were also carried out using carbon nanotubes and graphene, as the matrices in positive ion mode. The low molecular weight compounds including amino acids, peptides, ginsenosides, oligosaccharides and nucleosides, which play crucial roles in

physiological and pathologic processes [32,33], were detected with the three matrices. The representative spectra are shown in Fig. 4 and Fig. S2. As shown in Fig. 4a and Fig. S2b and S2c, there were strong interference ions caused by graphene and carbon nanotubes matrices, which were due to the cluster ionization of graphene and carbon nanotubes matrices. In contrast, MSNPs showed the mass spectra (Fig. 4a and Fig. S2a) of the clearly detected amino acid at *m/z* 169.12 and 185.09 as well as leu-enkephalin at *m/z* 578.27, 594.24, and 616.24 with no background ion interferences. For analysis of compounds with molecular weights above 700 daltons, ginsenoside Rg2 was taken as an example (Fig. S2d-f). In contrast, more background ions and lower signal intensity were obtained using graphene (Fig. S2e) and carbon nanotubes as matrices (Fig. S2f), respectively.

In short, MSNPs exhibited outstanding matrix properties such as high homogeneity of crystallization, low noise, and better salt tolerance. These behaviors are prerequisite for further investigation.

**Softer ionization of MSNP matrix for small molecule analysis**

Although MALDI is generally considered to be a soft ionization technique, the observation of fragments in nanostructure-assisted laser desorption/ionization or MALDI–especially at higher laser energies–has been previously reported [24,27,34]. To confirm the ability of MSNP for non-destructive analysis of labile compounds, two nonreducing oligosaccharides (raffinose (Gal(1→6)Glc(1→2)Fru), sucrose (Glc(1→2)Fru),) and 2′-deoxycytidine, which are regarded as labile species [34,35], were selected as model analytes. The ion at *m/z* 203.06 (Fig. 4b) has the highest

intensity, belonging to the loss of one hexose residue (162 Da) from the intact molecular ions of sucrose using graphene and carbon nanotubes as matrices. Two consecutive hexose residue losses from the sodium- and potassium-adducted raffinose ions due to the glycosidic bond cleavage, i.e., *m/z* 365.12, 381.09 (M – 162) and 203.06 (M – 162 × 2), are observed in Fig. 4c (pink and blue spectra). In contrast, MSNP-assisted LDI MS is able to produce the intact molecular ions with little or even no fragmentation as displayed in the orange spectra in Fig. 4b and c under the same laser energy, which is ascribed to the very homogenous surface without large clusters.

To confirm the above results, 2′-deoxycytidine was also analyzed with SALDI TOF MS using carbon nanotubes, graphene, and MSNPs as matrices. As shown in Fig. 4d (pink and blue spectra), high degree of fragmentation ions of 2′-deoxycytidine, such as the peaks of *m/z* at 112.07 ($[cytosine + H]^+$), 134.06 ($[cytosine + Na]^+$), 150.03 [cytosine + $K]^+$, 156.05 ($[cytosine + 2Na - H]^+$), and 172.04 ($[cytosine + Na + K - H]^+$), were observed, which were caused by the glycosidic bond cleavage (C-N) of 2′-deoxycytidine (Fig. S3). With regard to MSNPs (orange spectrum in Fig. 4d), only one minor fragment ion at *m/z* 112.07 was observed, allowing us to quickly assign the quasimolecular ion. These results indicated that the MSNP matrix was a good candidate material in the SALDI-TOF-MS analysis of small molecules due to the absence of interference with matrix peaks and very soft ionization.

**Application to the analysis of WGOS in *Panax Ginseng* root**

To further evaluate the feasibility of MSNP matrix for robust applications, *Panax ginseng,* which is a traditional Chinese herb with a clinical record of anti-aging activity,

anti-diabetic activity, immunoregulatory activity, etc. [36], was investigated. Fig. 5 depicts the mass spectra of water-soluble ginseng monosaccharides (WGOS-1), water-soluble ginseng disaccharides (WGOS-2), and water-soluble ginseng trisaccharides (WGOS-3) obtained from a warm-water extract of *Panax ginseng* roots as we previously reported [37]. The common ions at *m/z* 219.03, 381.07, and 543.13 in Fig. 5 were assigned as potassium adduct ions of WGOS-1, WGOS-2, and WGOS-3, respectively. Sodiated WGOS-1 (*m/z* 203.06) and WGOS-2 (*m/z* 365.11) in Fig. 5b and sodiated WGOS-1 (*m/z* 203.06) in Fig. 5c were also observed. It is obvious that interference ions observed in the mass spectra of using carbon nanotubes and graphene as matrices were completely eliminated in MSNP-assisted LDI MS (Fig. 5a), generating a clean background.

The relative abundances of WGOS-1, WGOS-2, and WGOS-3 vary greatly from one spectrum to another (Fig. 5a-c). WGOS-3 ions at m/z 543.13 almost disappeared and WGOS-1 ions were base peaks using graphene (Fig. 5b) and carbon nanotubes (Fig. 5c) matrices. In MSNP-assisted LDI MS (Fig. 5a), the relative abundance rank, from the highest to the lowest, was in the order WGOS-2 > WGOS-3 > WGOS-1. On the basis of the results mentioned above, i.e. that abundant fragmentation ions were detected for nonreducing oligosaccharides using graphene and carbon nanotubes matrices (Fig. 4b and c), it can be inferred that the relatively “hard” ionization of graphene and nanotubes matrices lead to fragmentation of the analytes. The rank order of relative abundance was WGOS-1 >> WGOS-2 >> WGOS-3 (Fig. 5b and c). From these results, one can conclude that frequent false-positive results may occur in mixtures analyzed by

graphene and carbon nanotubes-assisted LDI MS. Measurements using MSNPs as matrices reflect the actual ratios of the components in the sample solutions [37] and are therefore of substantial analytical value.

Although MSNP matrix has been used with great success, it suffers from some drawbacks. A major constraint is that the signal intensities are relatively low in MSNP-assisted LDI MS. Additionally, similar with other inorganic matrices, MSNP is not a suitable matrix to analyze macromolecules.

**Conclusion**

MSNPs were synthesized and employed as novel matrices for small biomolecule analysis by positive ion SALDI TOF MS. A wide range of small biomolecules including oligosaccharides, amino acids, peptides, nucleosides, and ginsenosides were investigated. The comparison between MSNPs and conventional nanometer materials revealed that NSNPs resulted in little or no fragmentation during analysis of labile compounds including sucrose, raffinose, and 2′-deoxycytidine. The difficulties in differentiating the quasimolecular ions from the fragment ions that are often encountered in conventionally nanostructure-assisted LDI MS are eliminated by using the soft matrix. The practical application of this soft matrix is further demonstrated by the successful analysis of the water-soluble ginseng extract. The limitation of this method is that macromolecules cannot be detected in MSNP-assisted LDI MS. In summary, the new MSNP matrix is a valid tool for solving the analytical challenges such as small biomolecular detection, reproducibility, and fragmentation in MALDI TOF MS.

**Acknowledgments** This work was supported by the Science and Technology Development Planning Project of Jilin Province (no. 20170623026TC, 20160101220JC, 20160204027YY, 201603080YY), and the Health Technology Innovation Project of Jilin Province (no. 2016J098).

**Compliance with ethical standards** The authors declare that they have no competing interests.

**References**

1. Scott DE, Bayly AR, Abell C, Skidmore J (2016) Small molecules, big targets: drug discovery faces the protein-protein interaction challenge. Nat Rev Drug Discovery 15:533−550. https://doi.org/10.1038/nrd.2016.29
2. May M (2015) Synthetic biology's clinical applications. Science 349:1564−1566. https://doi.org/10.1126/science.349.6255.1564
3. Wolan DW, Zorn JA, Gray DC, Wells JA (2009) Small-molecule activators of a proenzyme. Science 326:853−858. https://doi.org/10.1126/science.1177585
4. Lubin A, De Vries R, Cabooter D, Augustijns P, Cuyckens FJ (2017) An atmospheric pressure ionization source using a high voltage target compared to electrospray ionization for the LC/MS analysis of pharmaceutical compounds. Pharm Biomed Anal 142:225–231. https://doi.org/10.1016/j.jpba.2017.05.003
5. Evans AM, DeHaven CD, Barrett T, Mitchell M, Milgram E (2009) Integrated, nontargeted ultrahigh performance liquid chromatography/electrospray ionization tandem mass spectrometry platform for the identification and relative quantification of the small-molecule complement of biological systems. Anal Chem 81:6656−6667.

https://doi.org/10.1021/ac901536h

6. Yang HM, Wang JW, Song FR, Zhou YH, Liu SY (2011) Isoliquiritigenin (4,2',4'-trihydroxychalcone): a new matrix-assisted laser desorption/ionization matrix with outstanding properties for the analysis of neutral oligosaccharides. Anal Chim Acta 701:45−51. https://doi.org/10.1016/j.aca.2011.05.051
7. Bechara C, Bolbach G, Bazzaco P, Sharma KS, Durand G, Popot JL, Zito F, Sagan S (2012) MALDI-TOF mass spectrometry analysis of amphipol-trapped membrane proteins. Anal Chem 84:6128−6135. https://doi.org/10.1021/ac301035r
8. Yang HM, Liu N, Liu SY (2013) Determination of peptide and protein disulfide linkages by MALDI mass spectrometry. Top Curr Chem 331:79–116. https://doi.org/10.1007/128_2012_384
9. Abdelhamid HN (2017) Organic matrices, ionic liquids, and organic matrices@nanoparticles assisted laser desorption/ionization mass spectrometry. Trends Analyt Chem 89:68−98. https://dx.doi.org/10.1016/j.trac.2017.01.012
10. Abdelhamid HN, Wu HF (2013) Furoic and mefenamic acids as new matrices for matrix assisted laser desorption/ionization-(MALDI)-mass spectrometry. Talanta 115:442–450. https://dx.doi.org/10.1016/j.talanta.2013.05.050
11. van Kampen JJ, Burgers PC, de Groot R, Gruters RA, Luider TM (2011) Biomedical application of MALDI mass spectrometry for small-molecule analysis. Mass Spectrom Rev 30:101−120. https://doi.org/10.1002/mas.20268
12. Abdelhamid HN (2016) Ionic liquids for mass spectrometry: Matrices, separation and microextraction. Trends Analyt Chem 77:122−138.

https://doi.org/0.1016/j.trac.2015.12.007

13. Abdelhamid HN (2018) Nanoparticle assisted laser desorption/ionization mass spectrometry for small molecule analytes. Microchim Acta 185:200−215. https://doi.org/10.1007/s00604-018-2687-8

14. Sekuła J, Nizioł J, Rode W, Ruman T (2015) Gold nanoparticle-enhanced target (AuNPET) as universal solution for laser desorption/ionization mass spectrometry analysis and imaging of low molecular weight compounds. Anal Chim Acta 875:61–72. https://doi.org/10.1016/j.aca.2015.01.046

15. Hua PY, Manikandan M, Abdelhamid HN, Wu HF (2014) Graphene nanoflakes as an efficient ionizing matrix for MALDI-MS based lipidomics of cancer cells and cancer stem cells. J Mater Chem B 2:7334–7343. https://doi.org/10.1039/c4tb00970c

16. Shi CY, Deng CH (2016) Recent advances in inorganic materials for LDI-MS analysis of small molecules. Analyst 141:2816–2826. https://doi.org/10.1039/c6an00220j

17. Abdelhamid HN, Lin YC, Wu HF (2017) Thymine chitosan nanomagnets for specific preconcentration of mercury(II) prior to analysis using SELDI-MS. Microchim Acta 184:1517–1527. https://doi.org/10.1007/s00604-017-2125-3

18. Chen YS, Ding J, He XM, Xu J, Feng YQ (2018) Synthesis of tellurium nanosheet for use in matrix assisted laser desorption/ionization time-of-flight mass spectrometry of small molecules. Microchim Acta 185:368−376. https://doi.org/10.1007/s00604-018-2882-7

19. Abdelhamid HN, Wu BS, Wu HF (2014) Graphene coated silica applied for high ionization matrix assisted laser desorption/ionization mass spectrometry: A novel approach for environmental and biomolecule analysis. Talanta 126:27-37. https://doi.org/10.1016/j.talanta.2014.03.016

20. Kailasa SK, Wu HF (2013) Surface-assisted laser desorption-ionization mass spectrometry of oligosaccharides using magnesium oxide nanoparticles as a matrix. Microchim Acta 180:405−413. https://doi.org/10.1007/s00604-012-0933-z

21. Marsico AL, Duncan B, Landis RF, Tonga GY, Rotello VM, Vachet RW (2017) Enhanced laser desorption/ionization mass spectrometric detection of biomolecules using gold nanoparticles, matrix, and the coffee ring effect. Anal Chem 89:3009–3014. https://doi.org/10.1021/acs.analchem.6b04538

22. Phan NT, Mohammadi AS, Pour MD, Ewing AG (2016) Laser desorption ionization mass spectrometry imaging of drosophila brain using matrix sublimation versus modification with nanoparticles. Anal Chem 88:1734−1741. https://doi.org/10.1021/acs.analchem.5b03942

23. Spencer MT, Furutani H, Oldenburg SJ, Darlington TK, Prather KA (2008) Gold nanoparticles as a matrix for visible-wavelength single-particle matrix-assisted laser desorption/ionization mass spectrometry of small biomolecules. J Phys Chem C 112:4083–4090. https://doi.org/0.1021/jp076688k

24. Liang QL, Macher T, Xu YL, Bao YP, Cassady CJ (2014) MALDI MS in-source decay of glycans using a glutathione-capped iron oxide nanoparticle matrix. Anal Chem 86:8496−8503. https://doi.org/10.1021/ac502422a

25. Warren AD, Conway U, Arthur CJ, Gates PJ (2016) Investigation of colloidal graphite as a matrix for matrix ‐ assisted laser desorption/ionisation mass spectrometry of low molecular weight analytes. J Mass Spectrom 51:491–503. https://doi.org/10.1002/jms.3774

26. Wei J, Buriak JM, Siuzdak G (1999) Desorption–ionization mass spectrometry on porous silicon. Nature 399:243–246. https://doi.org/10.1038/20400

27. Go EP, Apon JV, Luo G, Saghatelian A, Daniels RH, Sahi V, Dubrow R, Cravatt BF, Vertes A, Siuzdak G (2005) Desorption/ionization on silicon nanowires. Anal Chem 77:1641–1646. https://doi.org/10.1021/ac048460o

28. Shao MF, Ning FY, Zhao JW, Wei M, Evans DG, Duan X (2012) Preparation of Fe3O4@SiO2@layered double hydroxide core-shell microspheres for magnetic separation of proteins. J Am Chem Soc 134:1071–1077. https://doi.org/10.1021/ja2086323

29. Tietze R, Zaloga J, Unterweger H, Lyer S, Friedrich RP, Janko C, Pöttler M, Dürr S, Alexiou C (2015) Magnetic nanoparticle-based drug delivery for cancer therapy. Biochem Biophys Res Commun 468:463–470. https://doi.org/10.1016/j.bbrc.2015.08.022

30. Im SH, Herricks T, Lee YT, Xia YN (2005) Synthesis and characterization of monodisperse silica colloids loaded with superparamagnetic iron oxide nanoparticles. Chem Phys Lett 401:19–23. https://doi.org/10.1016/j.cplett.2004.11.028

31. Zou ZQ, Ibisate M, Zhou Y, Aebersold R, Xia YN, Zhang H (2008) Synthesis and

evaluation of superparamagnetic silica particles for extraction of glycopeptides in the microtiter plate format. Anal Chem 80:1228–1234. https://doi.org/10.1021/ac701950h

32. Wang JN, Qiu SL, Chen SM, Xiong CQ, Liu HH, Wang JY, Zhang N, Hou J, He Q, Nie ZX (2015) MALDI-TOF MS imaging of metabolites with a N-(1-Naphthyl) ethylenediamine dihydrochloride matrix and its application to colorectal cancer liver metastasis. Anal Chem 87:422–430. https://doi.org/10.1021/ac504294s
33. Chen YL, Gao D, Bai HR, Liu HX, Lin S, Jiang YY (2016) Carbon dots and 9AA as a binary matrix for the detection of small molecules by matrix-assisted laser desorption/ionization mass spectrometry. J Am Soc Mass Spectrom 27:1227–1235. https://doi.org/10.1007/s13361-016-1396-y
34. Yang HM, Li ZJ, Wan DB, Lian WH, Liu SY (2013) Identification of reducing and nonreducing neutral carbohydrates by laser-enhanced in-source decay (LEISD) MALDI MS. J Mass Spectrom 48: 539–543. https://doi.org/10.1002/jms.3202
35. Yang HM, Wan DB, Song FR, Liu ZQ, Liu SY (2013) Argon direct analysis in real time mass spectrometry in conjunction with makeup solvents: a method for analysis of labile compounds. Anal Chem 85:1305–1309. https://doi.org//10.1021/ac3026543
36. Ru WW, Wang DL, Xu YP, He XX, Sun YE, Qian LY, Zhou XS, Qin YF (2015) Chemical constituents and bioactivities of Panax ginseng (C. A. Mey.). Drug Discov Ther 9:23–32. https://doi.org/10.5582/ddt.2015.01004
37. Wan DB, Jiao LL, Yang HM, Liu SY (2012) Structural characterization and

immunological activities of the water-soluble oligosaccharides isolated from the Panax ginseng roots. Planta 235:1289–1297. https://doi.org/10.1007/s00425-011-1574-x

## Figure legends

**Fig. 1** Characterization of MSNPs: (a) Scanning electron microscopic image of MSNPs and (b) UV−vis absorption spectrum of the MSNPs dispersion.

**Fig. 2** (a) The optical image of MSNPs and raffinose co-crystal by the sample-first method. (b) Calibration plots for quantitative analysis of berberine and palmatine by SALDI-TOF MS with MSNPs. Every dot is the average of 5 mass spectra, and each spectrum is accumulated from 500 laser shots total.

**Fig. 3** SALDI mass spectra of a mixture of glutamine (M1, MW = 146.07 Da), glucose (M2, MW = 180.06 Da), 2′-deoxycytidine (M3, MW = 227.09 Da), carbetamide (M4, MW = 236.12 Da), a dipeptide (Asp-Leu, DL) (M5, MW = 246.25 Da), and kojibiose (M6, MW = 342.12 Da) using MSNPs as matrix in the presence of different types of salts: (a) 2 M NaCl, (b) 2 M $NH_4HCO_3$, and (c) 2 M urea in positive ion mode at 80% laser energy.

**Fig. 4** SALDI mass spectra of (a) lysine (10 ppm, *m/z* 169.12, $[M + Na]^+$; *m/z* 185.09, $[M + K]^+$; *m/z* 191.11, $[M + 2Na - H]^+$), (b)sucrose (50 ppm, *m/z* 365.12, $[M + Na]^+$; *m/z* 381.09, $[M + K]^+$), (c) raffinose (50 ppm, *m/z* 527.14, $[M + Na]^+$; *m/z* 543.11, $[M + K]^+$), and (d) 2′-deoxycytidine (5 ppm, *m/z* 250.09, $[M + Na]^+$; *m/z* 260.06, $[M + K]^+$) by using carbon nanotubes (pink), graphene (blue), and MSNPs (orange) matrices in positive ion mode at 70% laser energy. The asterisks mark matrix peaks in the spectra.

**Fig. 5** SALDI mass spectra of WGOS-1, WGOS-2, and WGOS-3 obtained from a warm-water extract of *Panax ginseng* roots using (a) MSNPs, (b) graphene, and (c) carbon nanotubes matrices in positive ion mode at 70% laser energy.

**Fig. 1**

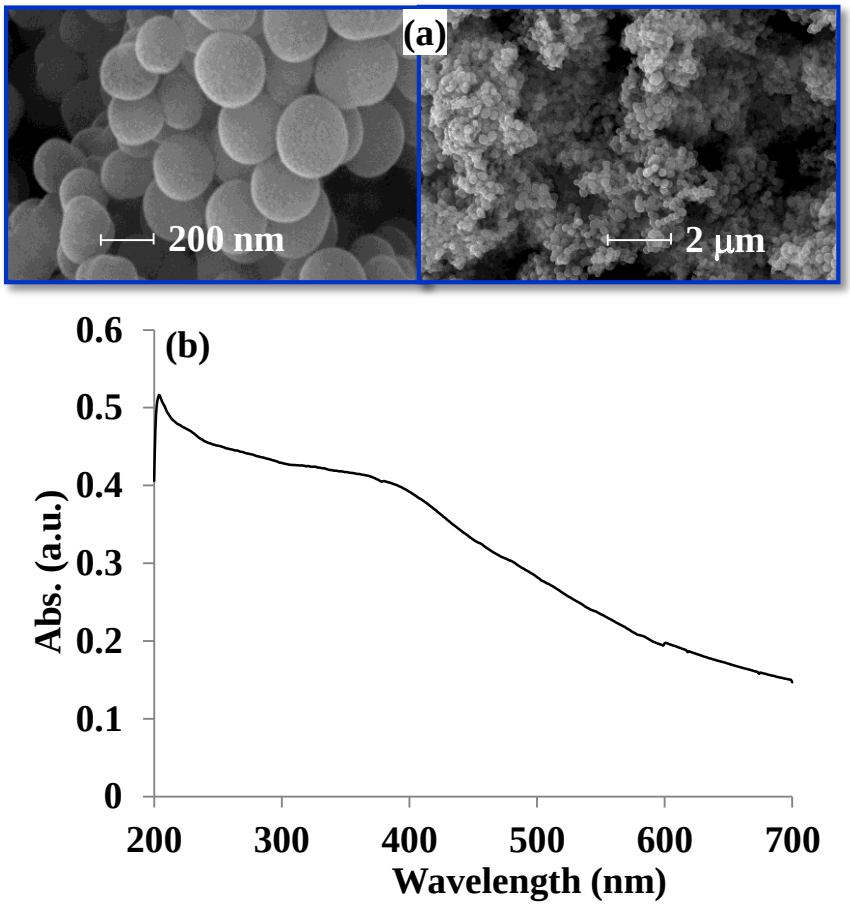
(a)
200 nm
2 μm
(b)
Abs. (a.u.)
0.6
0.5
0.4
0.3
0.2
0.1
0
200
300
400
500
600
700
Wavelength (nm)

**Fig. 2**

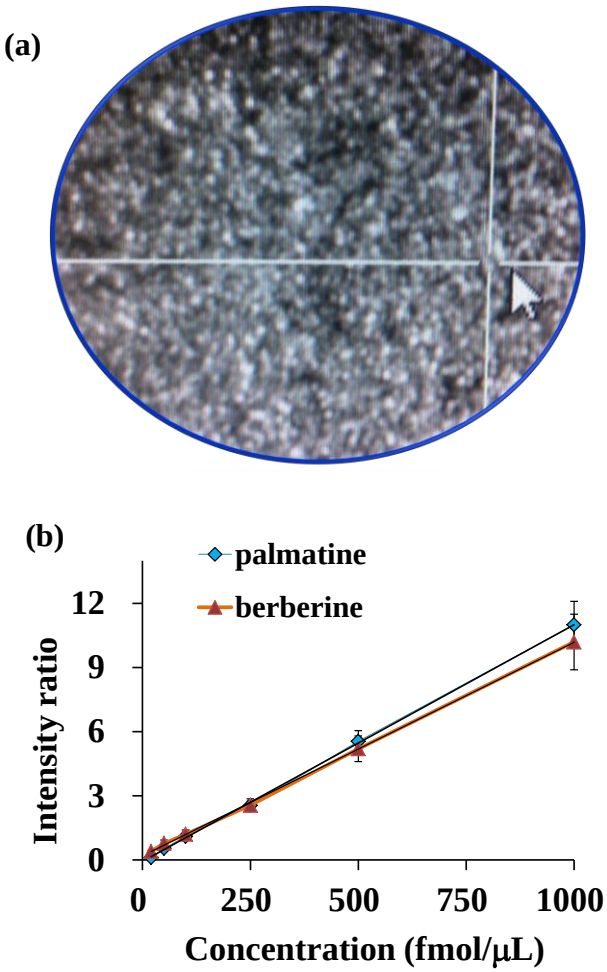
(a)
(b)
palmatine
berberine
Intensity ratio
12
9
6
3
0
0
250
500
750
1000
Concentration (fmol/μL)

**Fig. 3**

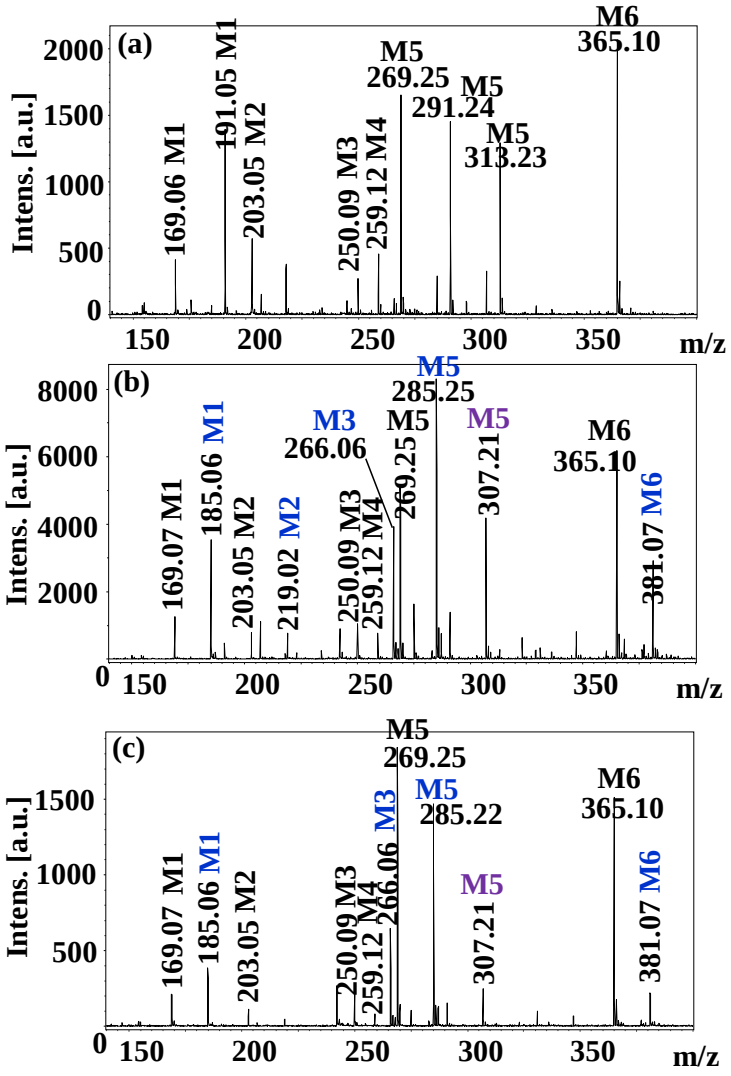
(a)
Intens. [a.u.]
2000
1500
1000
500
0
150
200
250
300
350
m/z
169.06 M1
191.05 M1
203.05 M2
250.09 M3
259.12 M4
M5
269.25
M5
291.24
M5
313.23
M6
365.10
(b)
Intens. [a.u.]
8000
6000
4000
2000
0
150
200
250
300
350
m/z
169.07 M1
185.06 M1
203.05 M2
219.02 M2
M3
266.06
250.09 M3
259.12 M4
M5
269.25
M5
285.25
M5
307.21
M6
365.10
381.07 M6
(c)
Intens. [a.u.]
1500
1000
500
0
150
200
250
300
350
m/z
169.07 M1
185.06 M1
203.05 M2
250.09 M3
259.12 M4
M3
266.06
M5
269.25
M5
285.22
M5
307.21
M6
365.10
381.07 M6

**Fig. 4**

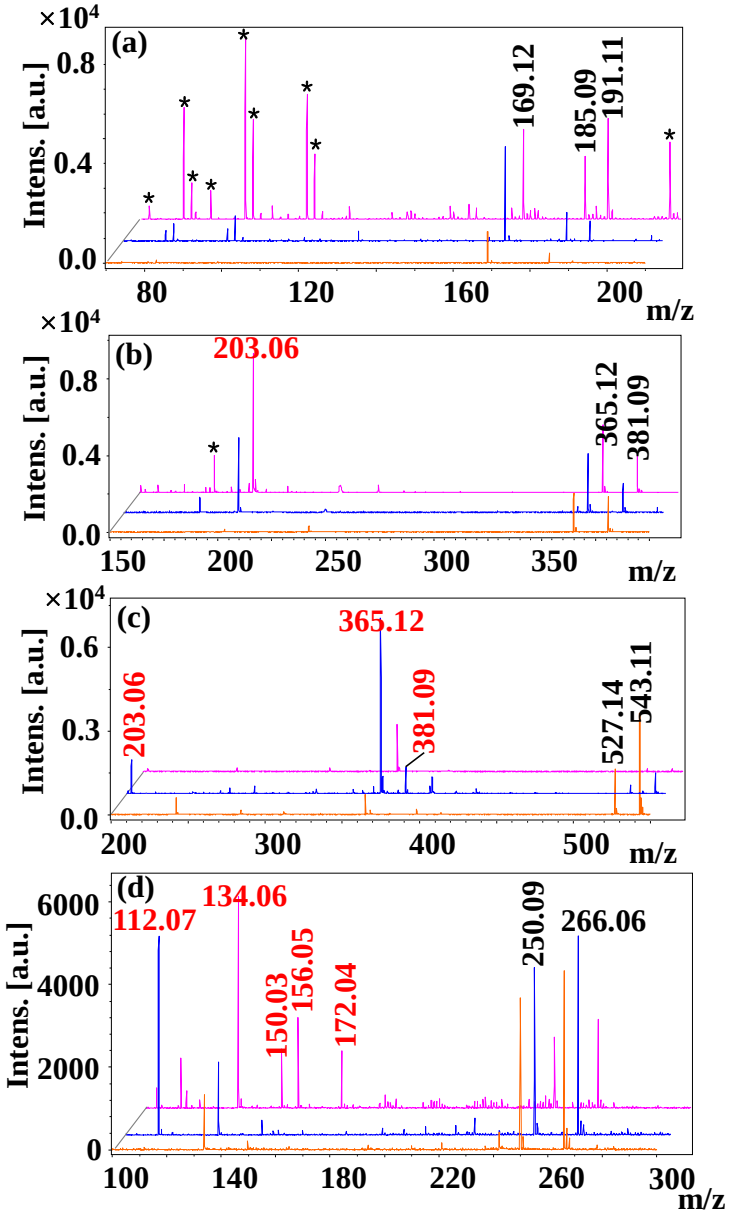
(a)
×10^4
Intens. [a.u.]
0.8
0.4
0.0
169.12
185.09
191.11
80
120
160
200
m/z
(b)
203.06
365.12
381.09
150
200
250
300
350
(c)
365.12
203.06
381.09
527.14
543.11
0.6
0.3
200
300
400
500
(d)
134.06
112.07
150.03
156.05
172.04
250.09
266.06
6000
4000
2000
0
100
140
180
220
260
300

**Fig. 5**

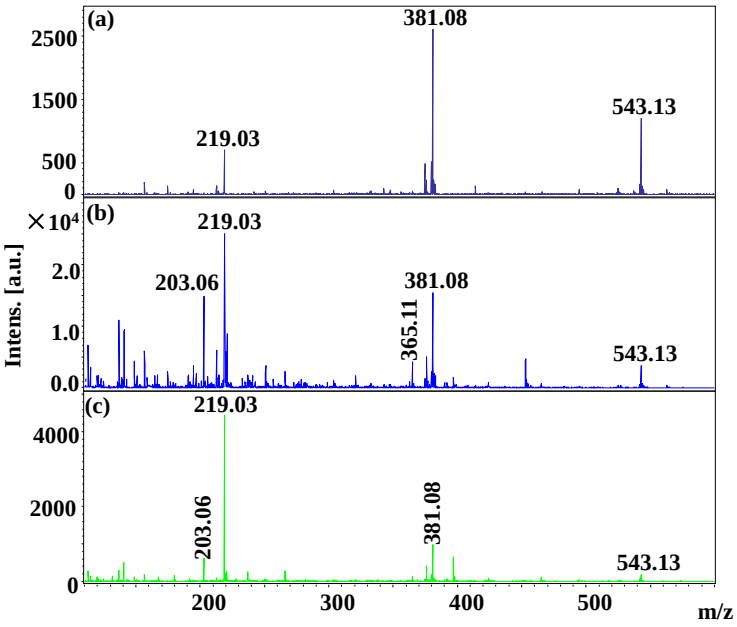
(a)
381.08
543.13
219.03
2500
1500
500
0
(b)
219.03
203.06
381.08
365.11
543.13
×10⁴
2.0
1.0
0.0
(c)
219.03
203.06
381.08
543.13
4000
2000
0
Intens. [a.u.]
200
300
400
500
m/z